An Enhanced Proprioceptive Method for Soft Robots Integrating Bend Sensors and IMUs

Dong Heon Han, Mayank Mehta, Runze Zuo, Zachary Wanger, Daniel Bruder

Abstract—This study presents an enhanced proprioceptive method for accurate shape estimation of soft robots using only off-the-shelf sensors, ensuring cost-effectiveness and easy applicability. By integrating inertial measurement units (IMUs) with complementary bend sensors, IMU drift is mitigated, enabling reliable long-term proprioception. A Kalman filter fuses segment tip orientations from both sensors in a mutually compensatory manner, improving shape estimation over single-sensor methods. A piecewise constant curvature model estimates the tip location from the fused orientation data and reconstructs the robot's deformation. Experiments under no loading, external forces, and passive obstacle interactions during 45 minutes of continuous operation showed a root mean square error of 16.96 mm (2.91% of total length), a 56% reduction compared to IMUonly benchmarks. These results demonstrate that our approach not only enables long-duration proprioception in soft robots but also maintains high accuracy and robustness across these diverse conditions.

Index Terms—Soft sensors and actuators

I. INTRODUCTION

Soft robots possess intrinsic compliance and virtually infinite degrees of freedom, enabling continuous deformation [1]. To leverage these characteristics for safe and adaptive interaction in dynamic environments, proprioception—the ability to sense body configuration—is essential [2]. However, achieving accurate proprioception remains challenging due to material flexibility and complex nonlinear deformation [3]. Reliable proprioception is thus critical for enabling stable motion planning and control in soft robotic systems.

Various transducers—resistive [4], capacitive [5], inductive [6], magnetic [7], and optical [8]—have been used for shape awareness in soft robots, often integrated into electronic skins [9]. Yet, these require specialized fabrication, limiting accessibility. Recent works show that off-the-shelf sensors can offer simpler, low-cost alternatives for shape estimation. Among such sensors, IMUs are popular for their compactness, ease of integration, and real-time tracking. Martin et al. [10] combined multiple IMUs with an extended PCC model [11], identifying IMU drift as a limitation. Our method introduces a bendsensor reference to correct IMU vaw drift before Kalman fusion, improving long-duration stability. Peng et al. [12] validated a tendon-driven manipulator with multiple IMUs but did not address drift. Stella et al. [13] used a kinematicsbased filter with IMU orientation data but assumed negligible twist, restricting motion to planar bending. While this simplification reduces computation, it limits robustness under

The authors are with the Mechanical Engineering Department at the University of Michigan, Ann Arbor, MI 48109, USA {dongheon, mayanknm, zuorunze, zwanger, bruderd}@umich.edu

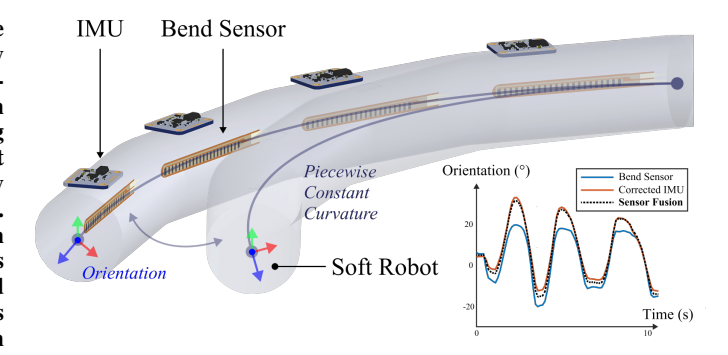


Fig. 1. Overview of our proposed proprioceptive sensing method for soft robots using off-the-shelf IMUs and bend sensors. Shape estimation is based on a piecewise constant curvature model using segment-tip orientations. IMU drift is corrected using bend-sensor references before fusion, enabling 45-minute continuous operation.

torsional impact, unlike our method which handles coupled bending-twisting deformation. Transient accelerations further amplify IMU noise and drift accumulation [14], degrading accuracy in long-term operation.

To mitigate drift, previous studies fused IMUs with cameras [15] or draw-wire sensors [16]. However, camera-based fusion is affected by occlusion and lighting, and draw-wire methods require constant tension, introducing errors under compression. While such methods improve short-term accuracy, few demonstrate stable long-term drift correction under dynamic loads. Bend sensors offer an attractive alternative [17], providing direct deformation measurement unaffected by lighting or tension. Although noisy and hysteretic, they exhibit minimal drift and insensitivity to acceleration spikes, capturing real structural changes. Yet, off-the-shelf bend sensors have not been systematically exploited to suppress IMU drift or sustain long-duration proprioception. Our approach addresses this gap by using bend sensors as low-frequency references that anchor IMU drift within a two-stage fusion pipeline for reproducible, long-term accuracy.

The Kalman filter (KF) remains a standard tool for realtime sensor fusion, combining probabilistic modeling with prediction-correction cycles [18]. It is particularly effective for complementary fusion, integrating heterogeneous sensors [19]. However, its performance depends on accurate noise and covariance initialization, which is difficult in soft robots due to nonlinear material behavior [20]. Empirical calibration and data-driven approaches have therefore been used to model sensor deformation and improve estimation accuracy [21], [22]. Building on these insights, we empirically tune KF noise and covariance parameters to capture soft-robot nonlinearities, enhancing proprioceptive performance.

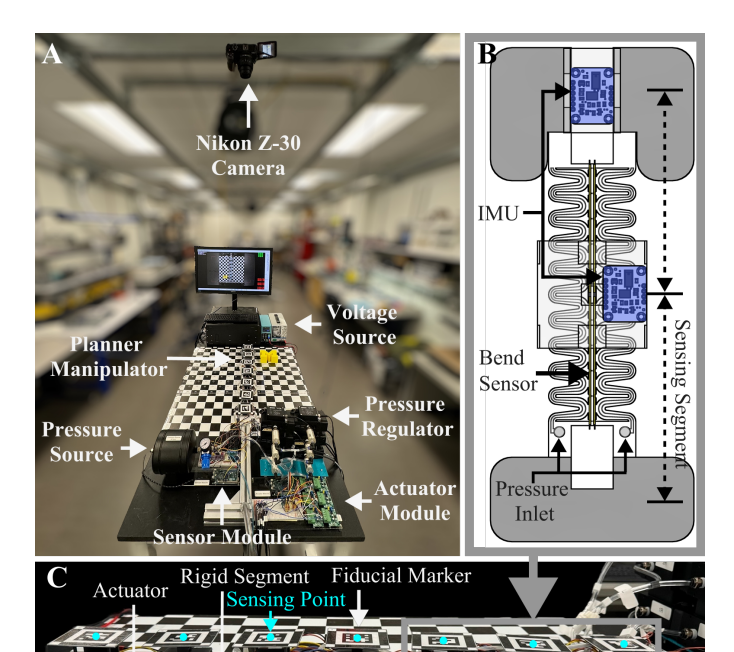


Fig. 2. Experimental setup for validating the sensing method. (A) Planar robot test rig. (B) Nth link with two actuators, four bend sensors (yellow), and two IMUs (blue) located between parallel sensors. (C) Full robot showing fiducial markers and sensing points for output comparison.

We propose a shape estimation framework using two off-the-shelf sensors: an IMU (BNO055, Bosch, Adafruit) and a bend sensor (2.2" Flex Sensor, Spectra Symbol), as shown in Fig. 1. Drift correction is first applied by comparing IMU and bend readings, followed by KF fusion for refined estimation. A PCC model maps orientation to shape, and KF parameters are optimized by minimizing RMSE against ground truth. We validate the approach on a 2D planar manipulator, where yaw drift—parallel to gravity—is most pronounced, offering a controlled test before generalizing to 3D environments.

This paper's main contributions are threefold. First, a compensatory drift-correction scheme anchoring IMU yaw to a calibrated bend-sensor curvature reference. Second, a two-stage fusion of segment-tip orientation and PCC-mapped position using linear KFs, improving accuracy without added hardware. Third, a fully off-the-shelf, low-cost implementation validated for 45 minutes under no-load, load, and obstacle-contact conditions, achieving a 56% RMSE reduction versus an IMU-only PCC baseline while retaining real-time, embedded feasibility. The Methods section details the sensing and fusion design, the Experiments section presents validation procedures, and the Discussion and Conclusion interpret results and suggest future directions.

II. METHODS

A sensing segment is defined as the smallest unit in which multiple sensors collect data for deformation estimation. Each segment independently estimates its local state from these measurements. Proprioception is achieved using off-the-shelf IMUs and bend sensors to estimate the orientation of each

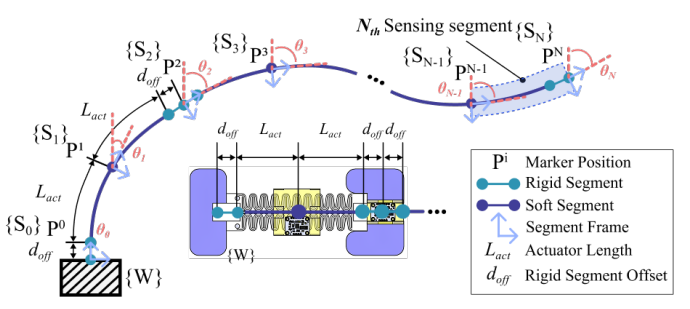


Fig. 3. A PCC kinematic model is used to map sensor readings to an estimate of the robot's shape. The robot is assumed to consists of a chain of rigid and constant curvature segments.

segment endpoint, as illustrated in Fig. 2. One end of the robot is fixed, and the structure bends laterally within a planar workspace. The bend sensor's resistance varies with curvature, exhibiting a bijective relationship between endpoint orientation difference and measured resistance determined through calibration (*V-Orient Map* in Fig. 4). To reduce noise and improve stability, two bend sensors are placed in parallel per segment, and their averaged output is used for orientation estimation, yielding both bend-sensor-mapped and IMU-derived orientations obtained from the IMU's onboard filter. As shown in Fig. 4, the sensing architecture integrates these measurements to estimate each segment's orientation and position. IMU drift is first corrected using the bendsensor reference (IMU Correction), and the corrected orientations are applied to the PCC model (PCC) for position estimation. Finally, the sensor outputs are fused through two Kalman filters—KF_{orient} for orientation and KF_{coord} for position—enhancing accuracy, suppressing noise, and ensuring stable proprioceptive performance.

A. Kinematics of Soft Manipulator

As shown in Figure 3, we choose to model the robot as a series of connected constant curvature segments. The robot consists of N sensing segments, each comprising a curvature with a length $L_{\rm act}$ and a rigid connector with an offset length $d_{\rm off}$. The i-th curvature C^i is expressed in the $\{S_i\}$ frame of each part as follows, where θ_i represents the angle of the curvature, and κ_i represents the radius of curvature:

$$C_{\{S_i\}}^i = \begin{bmatrix} \kappa_i \cdot (1 - \cos(\theta_i)) \\ \kappa_i \cdot \sin(\theta_i) \end{bmatrix} \quad \text{where} \quad \kappa_i = \frac{L_{\text{act}}}{\theta_i}$$
 (1)

 $R_{\{S_i\}}^i(\theta)$ represents the rotation matrix in the $\{S_i\}$ frame, and since the offset in each part can be attached either at the beginning or at the end, the *i*-th offset D^i of the rigid connector is expressed in two cases and is represented in the $\{S_i\}$ frame of each part as follows:

$$D_{\{S_i\}}^i = \begin{bmatrix} d_{\text{off}} \\ 0 \end{bmatrix} \cdot R_{\{S_i\}}^i(\theta) \quad \left(\theta = \begin{cases} \theta, & \text{if } i \text{ is odd} \\ 0, & \text{if } i \text{ is even} \end{cases}\right) \quad (2)$$

Finally, the end point in the $\{S_i\}$ frame is defined as $P_{\{S_i\}}^i$ as shown below (Figure 4):

$$P_{\{S_i\}}^i = C_{\{S_i\}}^i + D_{\{S_i\}}^i \tag{3}$$

The six points P_i represented in the $\{S_i\}$ frame can be transformed into the world frame $\{W\}$ as follows (*Frame to World*

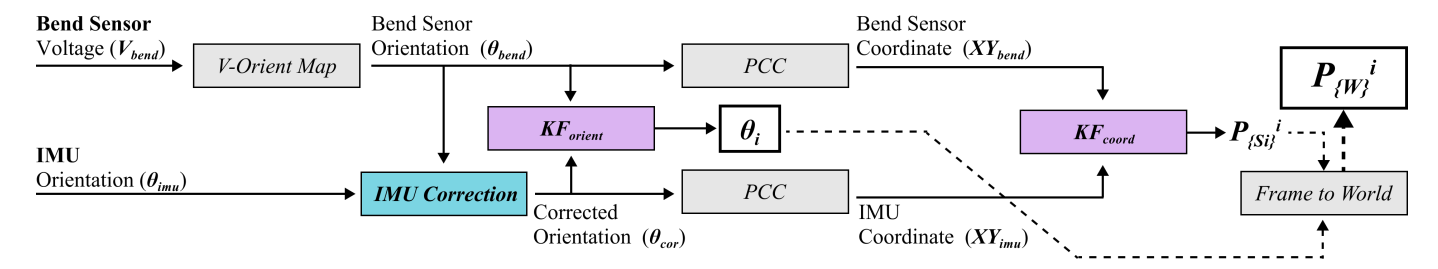


Fig. 4. Flowchart showing enhanced proprioception. The process starts with signals from the bend sensor and IMU, passes through an algorithm, and results in two output data: orientation in the S_i frame, θ^i , and position in the S_i frame, $P^i_{s_i}$, which are used to estimate the position of the end-effector. The orientation at each sensing point and the estimated end-effector position of each segment are then compared with the ground truth, denoted as $GT^i_{\theta\{S_i\}}$ and $GT^i_{P\{W\}}$, respectively, obtained from fiducial markers, and the RMSE is calculated based on the distance between the two positions.

from Figure 4):

$$\mathbf{P}_{\{W\}}^{i} = \left(\sum_{k=1}^{i-1} \mathbf{P}_{\{S_k\}}^{k} + \mathbf{P}_{\{S_i\}}^{i}\right) \cdot \prod_{k=1}^{i-1} \mathbf{R}_{\{S_k\}}^{k}(\theta)$$
(4)

B. IMU Drift Correction

IMU drift accumulates over time due to the integration of noise in gyroscopic angular velocity measurements. In contrast, calibrated bend sensors provide stable orientation estimates since they directly measure curvature and are less affected by cumulative errors. Drift is mitigated using a moving average filter with a defined window size and correction threshold. The offset is computed as the difference between the moving averages of IMU orientation (θ_{imu}) and bendsensor orientation (θ_{bend}) from Figure 4. When the offset exceeds the threshold, the IMU orientation is corrected by subtracting this value. This correction process (IMU Cor**rection** in Figure 4) is applied to all N IMUs to maintain consistent orientation accuracy. Although advanced onboard algorithms may further reduce long-term drift, fundamental sensor noise and nonlinearities limit purely computational solutions. By directly integrating bend-sensor data with IMU outputs, our method achieves real-time drift compensation, providing robust and reliable proprioception without additional algorithmic complexity.

C. Sensor Fusion Using Kalman Filter

We use linear Kalman filters for transparency and embedded suitability. The state evolves approximately linearly over small time steps. Nonlinearity is confined to the measurement mapping through PCC. We decouple orientation and mapped position to let each filter absorb different error sources. A KF is used to fuse IMU and bend sensor data for orientation θ_i and coordinates (x_i, y_i) in the $\{S_i\}$ frame (KF_{orient}) and KF_{coord} from Figure 4).

This process determines the orientation and position of all N segments, enabling overall robot shape estimation in the world frame, as illustrated in Figure 3. To model the decoupled estimation process, the system state vector is split into two separate components:

$$\hat{x}_{\text{orient}} = \begin{bmatrix} \theta_1 & \theta_2 & \dots & \theta_N \end{bmatrix}^T$$
 (5)

$$\hat{x}_{\text{coord}} = \begin{bmatrix} x_1 & y_1 & x_2 & y_2 & \dots & x_N & y_N \end{bmatrix}^T \tag{6}$$

Each of these state vectors is processed independently in the KF framework, depending on whether orientation or position is being estimated. As shown in Figure 4, estimating the shape of the robot requires two sequential steps:

- 1) The position of each segment's endpoint is estimated using the PCC model, which maps endpoint positions from both the IMU and bend sensor. The resulting x, y coordinates are then fused via a Kalman Filter (KF_{coord}).
- To reconstruct the robot's overall shape, the relative rotation of each segment is computed. Each segment's orientation from both sensors is fused using a Kalman Filter (KF_{orient}).

By combining both position and orientation estimations, the robot's full shape can be reconstructed accurately. The general form of the Kalman filter equations remains unchanged, but the state vector used depends on the specific estimation:

$$\hat{x}_{k|k-1} = A\hat{x}_{k-1|k-1} + Bu_k \tag{7}$$

$$P_{k|k-1} = AP_{k-1|k-1}A^T + Q (8)$$

followed by a Measurement Update Step.

$$K_k = P_{k|k-1}H^T \left(H P_{k|k-1}H^T + R \right)^{-1} \tag{9}$$

$$\hat{x}_{k|k} = \hat{x}_{k|k-1} + K_k \left(z_k - H \hat{x}_{k|k-1} \right) \tag{10}$$

Here, A denotes the state transition matrix, P_k the state covariance matrix, Q the process noise covariance representing system uncertainties, and R the measurement noise covariance reflecting sensor noise. The measurement matrix H maps sensor readings to the state vector with distinct components for each sensor. To enhance KF performance, Q, R, and H are optimized via gradient descent to minimize RMSE in both orientation and x-y position estimations. Each parameter is iteratively updated using the RMSE gradient, allowing the filter to adapt to variations in sensor reliability and system dynamics:

$$p_i \leftarrow p_i - \alpha \frac{\partial \text{RMSE}}{\partial p_i},$$
 (11)

where $p_i \in \{Q, R, H\}$ and α is the learning rate. During optimization, Q adjusts to system uncertainty, R is tuned per sensor to reflect noise characteristics, and H refines the sensorto-state mapping. This iterative process continues until the RMSE converges, ensuring accurate and robust KF estimates of both position and orientation. Per-cycle complexity scales

linearly with the number of segments, and the computational load remains low enough for real-time execution on a microcontroller-class platform, with latency primarily limited by sensor input/output rather than filtering computation.

III. EXPERIMENTS

A. Overview of the Planar Robot Test Rig

A planar soft robot was developed to validate the proposed sensing framework, comprising control, sensing, and camera modules. The control module regulates pneumatic pressure across three segments of the soft arm. As shown in Fig. 2, the arm consists of three 3D-printed thermoplastic elastomer (TPE) actuator modules, each used for configuration estimation. Each module integrates two kirigami-inspired actuators [23] that bend bidirectionally under pneumatic pressure. Modules are connected by 3D-printed PLA joints, and metal rollers at the base enable low-friction motion. Pressure regulators (Enfield TR series) driven by PWM-to-analog converters modulate a 280 kPa air supply, with a microcontroller generating PWM signals for actuation. The sensing module integrates bend sensors and IMUs, with each actuator module forming one sensing segment. Bend sensors are embedded in pre-printed spinal channels, and their analog outputs are multiplexed to an Arduino Due for acquisition from twelve sensors. Six IMUs communicate with the same microcontroller via an I²C expander. The camera module employs a ceilingmounted Nikon Z-30 to record the workspace. Enhanced ArUco markers [24] are placed at the IMU and bend-sensor locations to provide ground truth (GT) with 0.1 mm accuracy using OpenCV. A checkerboard background enables camera calibration via Zhang's method [25]. This setup provides highfidelity validation of the soft arm's real-time motion and configuration.

B. Training and Validation

Training data serve two purposes: (1) calibrating bendsensor readings to match the orientations of the sensing points (Figures 2 and 3), and (2) identifying optimal Kalman Filter (KF) parameters using bend-sensor orientations and driftcorrected IMU data. The dataset comprises 40,000 samples collected over approximately 4,000 s. Two-thirds are obtained by sweeping the robot $\pm 50^{\circ}$ for calibration, and the remaining third by generating randomized curvatures in each segment to ensure distinct actuator orientations (see accompanying video). All data are used exclusively for KF parameter optimization. Validation is conducted in three scenarios to test robustness against environmental variations, obstacles, and external forces. In **Scenario I**, the actuators swing the robot laterally without external loads. Scenario II applies external forces using a stick, and Scenario III places an obstacle at the center for collision and wrapping interactions. Scenarios II and III evaluate the impact of external disturbances on sensing performance. For each scenario, the effectiveness of the PCC model and KF-based fusion is assessed, identifying the method's strengths, limitations, and improvement areas. Performance is compared among four approaches: Fusion (IMU + bend via KF), **Bend** (bend-only), IMU_C (IMU corrected using bend data), and IMU_O (uncorrected IMU).

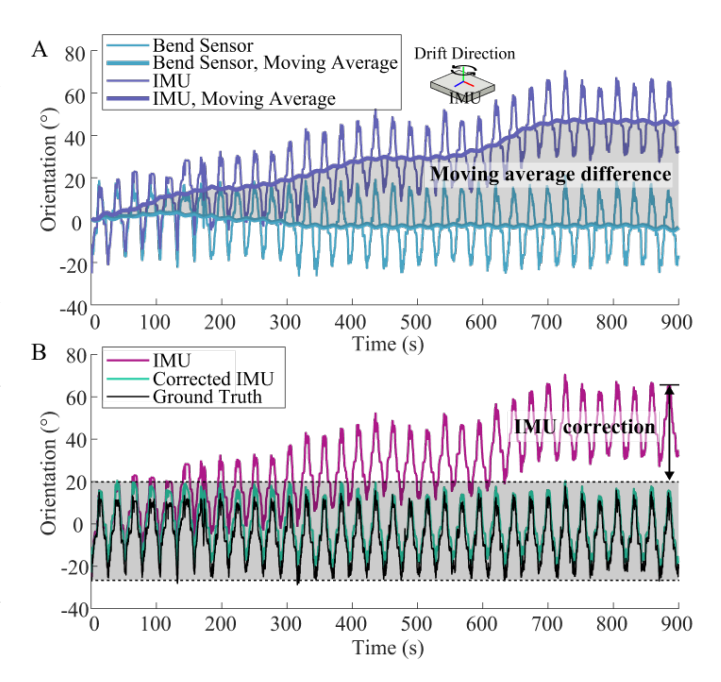


Fig. 5. IMU drift was observed over 900 seconds (15 minutes) while periodically changing the orientation of a sensing segment between -20 and 20 degrees. (A) The figure presents the orientation trend from the bend sensor and IMU using a moving average. The IMU error accumulates over time, indicating significant drift. (B) IMU correction results are compared to raw IMU values, demonstrating that the corrected IMU closely follows the ground truth.

IV. RESULTS

Each bend sensor is calibrated through voltage mapping and quadratic interpolation, yielding an average RMSE of 4.72° across 12 sensors. The mapped orientations serve as references for IMU drift correction. As shown in Figure 5, this process compensates approximately 45° of drift accumulated over 900 s (15 min), preventing divergence in the IMU signal. The plot represents one sensing segment, with similar results observed for the remaining five. A moving-average window of 100 samples and a correction threshold of 0.5° are used. Although demonstrated during periodic motion, this correction performs robustly across diverse movements. To assess estimation accuracy in Scenarios I-III (Figure 6, Table I), the error is defined as the Euclidean distance between the estimated xy end-effector position and the ground-truth fiducial marker. RMSE is then computed from these errors over a 45-min experiment, validating long-term reliability. In Table I, the first column aggregates results from S_I , S_{II} , and S_{III} . The Fusion method achieves the lowest RMSE of 16.96 mm (2.91) % of total arm length), demonstrating the highest accuracy. By comparison, Bend yields 24.62 mm (6.13 %), confirming the superiority of the fusion-based approach.

Using the method IMU_O yields the highest RMSE at 30.27 mm (5.20%), representing the poorest performance. For the method IMU_C , the RMSE is 17.68 mm (3.04%), performing slightly worse than the Fusion. When using method IMU_0 , the RMSE is 31.12 mm with an error percentage of 5.35%, which is better than the method $Bend_0$ but still falls short compared to methods using Fusion.

Scenario I: Fusion achieves the lowest RMSE of 10.97 mm

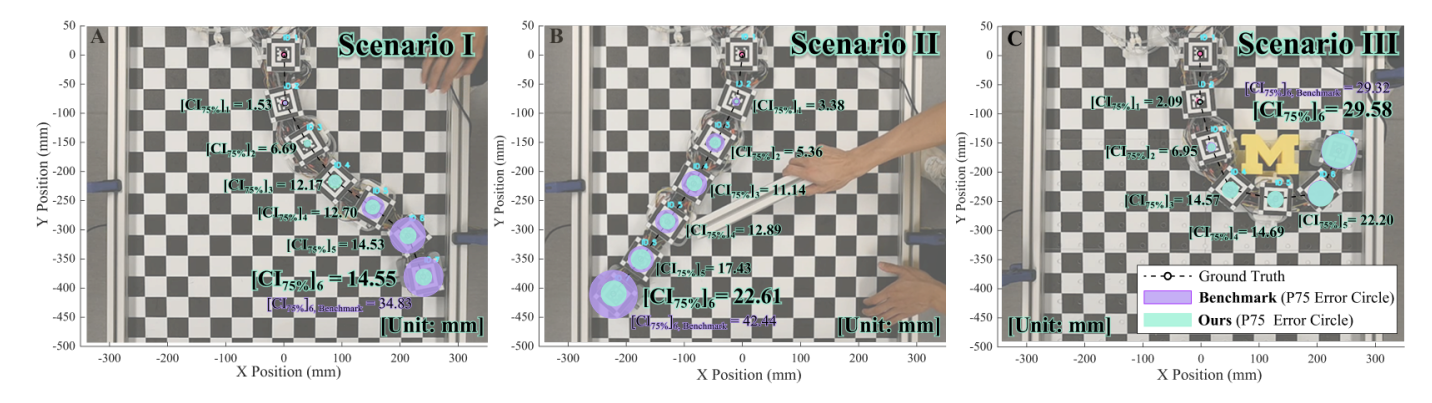


Fig. 6. We compare the estimations from Scenarios I, II, and III with the actual photos taken by the camera at those times. The diameter of the circles $([CI_{75\%}]_i)$ represents the error, defined as the Euclidean distance between the estimation from *Fusion* and the ground truth, indicating the error size within the 75th percentile. This is compared to the error of IMU_C , the benchmark $([CI_{75\%}]_{i,Benchmark})$.

TABLE I EXPERIMENTAL RMSE FOR DIFFERENT SCENARIO SETS

Methods	Scenario			
	$S_{I} \cup S_{II} \cup S_{III}$	S_{I}	S_{II}	S_{III}
Fusion	16.96 (2.91%)*	10.97 (1.89%)	20.24 (3.48%)	23.59 (4.05%)
Bend	24.62 (4.23%)	19.45 (3.34%)	30.10 (5.17%)	29.46 (5.06%)
IMU_C	17.68 (3.04%)	12.49 (2.15%)	21.88 (3.76%)	22.87 (3.93%)
IMU _O	30.27 (5.20%)	33.24 (5.71%)	36.68 (6.30%)	22.75 (2.19%)

The RMSE unit is millimeters (mm

(1.89%), followed by IMU_C at 12.49 mm (2.15%). Bend yields 19.45 mm (3.34%), and IMU_O produces the highest error at 33.24 mm (5.71%). **Scenario II:** Fusion again performs best with an RMSE of 20.24 mm (3.48%), followed by IMU_C at 21.88 mm (3.76%). Bend data results in 30.10 mm (5.17%), while IMU_O reaches the highest RMSE of 36.68 mm (6.30%). **Scenario III:** Fusion attains 23.59 mm (4.05%), while IMU_O slightly outperforms it with 22.75 mm (3.92%), representing the best performance in this case. IMU_C yields 22.87 mm (3.93%), and Bend exhibits the largest error at 29.46 mm (5.06%). Orientation errors mirror the position trends: the original IMU (IMU_O) shows increasing yaw bias, the drift-corrected IMU (IMU_C) removes low-frequency bias, and Fusion further reduces orientation variance across all segments.

V. DISCUSSION AND CONCLUSION

In this study, we presented an enhanced proprioceptive method using off-the-shelf sensors to improve the versatility and reliability of soft robots. Our goal was to establish an accurate sensing architecture effective across diverse scenarios and long durations. The complementary fusion of bend sensors and IMUs was shown to significantly improve estimation accuracy. Validation on a 2D planar robot confirmed the method's robustness in real time and demonstrated its potential for extension to 3D applications.

A. Key Findings and Performance Evaluation

IMU drift was effectively corrected using bend sensors (Fig. 5). The method remained stable over 45 min and is expected to scale to longer durations. This drift-correction strategy generalizes to 3D configurations, offering a simple

yet robust means of mitigating IMU drift. Bend sensors exhibited lower precision than IMUs due to resistive noise amplification, yielding higher uncertainty than IMU_C in all scenarios. While IMUs are less sensitive to vibration, they remain susceptible to drift, as observed in IMUO under prolonged motion or external acceleration (Scenarios I-II). In Fig. 6 and Table I, IMU_O unexpectedly outperforms Fusion in Scenario III. This anomaly arises from extreme passive deformation during obstacle contact, violating the constantcurvature assumption. Such conditions cause the PCC model to lose validity, degrading both bend-sensor calibration and KF tuning. Shorter segments or alternative curvature models may alleviate this limitation, while nonlinear or learning-based voltage-orientation mappings could improve extrapolation to large deformations. Outside such extremes, drift correction remains essential, and fusion of IMU_C with Bend consistently preserves high accuracy. KF gain balance depends on sensornoise estimation: overestimating bend-sensor noise biases toward the IMU, whereas underestimation increases overcorrection. Paired bend sensors reduce variance, and a thresholded drift anchor prevents transient instability. Figures 6-7 summarize performance across Scenarios I-III. Compared with Martin et al. [10], which fuses multiple IMUs via PCC modeling, the proposed method achieves the primary error reduction through drift correction, with further improvement from subsequent fusion. Although residual outliers appear during extreme deformations, overall RMSE decreases by 56%, yielding a 2.91% length-normalized error sustained for 45 min without vision or custom sensors—demonstrating reliable, low-cost proprioception.

B. Future Directions

Our study validated the feasibility of sensor fusion in planar soft robots, and the next stage is extending this framework to 3D deformation. Current commercial bend sensors are single-axis; thus, full 3D bending requires either integrating multiple uniaxial sensors as structural elements or replacing them with multi-axis curvature transducers. This modification would be purely structural—no change to the fusion algorithm is needed, as the existing architecture naturally generalizes to three dimensions. The system would remain real time,

^{*} The percentages represent the RMSE as a fraction of the total length of the manipulator.

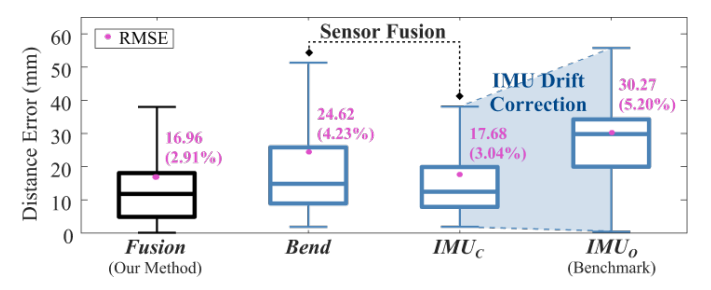


Fig. 7. The figure shows the RMSE (Root Mean Square Error) of the end-effector's Euclidean distance error for Scenario I,II,III across different estimation methods. Each box plot represents the distribution of errors for a specific method, with the box spanning from the 25th percentile (Q1) to the 75th percentile (Q3), and the horizontal line within each box indicating the median (50th percentile). The stars indicate the corresponding RMSE values for each method.

vision free, and robust against occlusion and lighting, ideal for embedded and wearable platforms with limited computation and power. Computation scales linearly with segment count, and local drift correction ensures scalability for longer or more articulated robots. Accuracy for complex configurations can be enhanced by shortening segments or adopting non-PCC curvature models. IMU drift is continuously compensated by bend-sensor references, while long-term effects of sensor aging only affects voltage-to-orientation calibration and can be corrected by periodic recalibration.

REFERENCES

- [1] D. Rus and M. T. Tolley, "Design, fabrication and control of soft robots," *Nature*, vol. 521, no. 7553, pp. 467–475, May 2015.
- [2] G. Soter, A. Conn, H. Hauser, and J. Rossiter, "Bodily aware soft robots: integration of proprioceptive and exteroceptive sensors," in 2018 IEEE international conference on robotics and automation (ICRA). IEEE, 2018, pp. 2448–2453.
- [3] R. K. Kramer, C. Majidi, R. Sahai, and R. J. Wood, "Soft curvature sensors for joint angle proprioception," in 2011 IEEE/RSJ International Conference on Intelligent Robots and Systems. IEEE, 2011, pp. 1919– 1926.
- [4] C. Della Santina, R. L. Truby, and D. Rus, "Data-driven disturbance observers for estimating external forces on soft robots," *IEEE Robotics* and automation letters, vol. 5, no. 4, pp. 5717–5724, 2020.
- [5] A. Tairych and I. A. Anderson, "Capacitive stretch sensing for robotic skins," *Soft robotics*, vol. 6, no. 3, pp. 389–398, 2019.
- [6] W. Felt, M. J. Telleria, T. F. Allen, G. Hein, J. B. Pompa, K. Albert, and C. D. Remy, "An inductance-based sensing system for bellows-driven continuum joints in soft robots," *Autonomous robots*, vol. 43, pp. 435– 448, 2019.
- [7] M. D. Mitchell, F. E. Hurley, and C. D. Onal, "Fast probabilistic 3-d curvature proprioception with a magnetic soft sensor," in 2021 IEEE 17th International Conference on Automation Science and Engineering (CASE). IEEE, 2021, pp. 215–220.
- [8] K. C. Galloway, Y. Chen, E. Templeton, B. Rife, I. S. Godage, and E. J. Barth, "Fiber optic shape sensing for soft robotics," *Soft robotics*, vol. 6, no. 5, pp. 671–684, 2019.
- [9] B. Shih, D. Shah, J. Li, T. G. Thuruthel, Y.-L. Park, F. Iida, Z. Bao, R. Kramer-Bottiglio, and M. T. Tolley, "Electronic skins and machine learning for intelligent soft robots," *Science Robotics*, vol. 5, no. 41, p. eaaz9239, 2020.
- [10] Y. J. Martin, D. Bruder, and R. J. Wood, "A proprioceptive method for soft robots using inertial measurement units," in 2022 IEEE/RSJ International Conference on Intelligent Robots and Systems (IROS). IEEE, 2022, pp. 9379–9384.
- [11] R. J. Webster III and B. A. Jones, "Design and kinematic modeling of constant curvature continuum robots: A review," *The International Journal of Robotics Research*, vol. 29, no. 13, pp. 1661–1683, 2010.
- [12] R. Peng, Y. Wang, and P. Lu, "A tendon-driven continuum manipulator with robust shape estimation by multiple imus," *IEEE Robotics and Automation Letters*, 2024.

- [13] F. Stella, C. Della Santina, and J. Hughes, "Soft robot shape estimation with imus leveraging pcc kinematics for drift filtering," *IEEE Robotics* and Automation Letters, 2023.
- [14] R. Rong and C. Kuo, "Dynamic soft tissue artifacts during impulsive loads: Measurement errors vary with wearable inertial measurement unit sensor design," *IEEE Transactions on Biomedical Engineering*, 2024.
- [15] H. Bezawada, C. Woods, and V. Vikas, "Shape reconstruction of soft manipulators using vision and imu feedback," *IEEE Robotics and Automation Letters*, vol. 7, no. 4, pp. 9589–9596, 2022.
- [16] K. Stewart, Z. Qiao, and W. Zhang, "State estimation and control with a robust extended kalman filter for a fabric soft robot," *IFAC-PapersOnLine*, vol. 55, no. 37, pp. 25–30, 2022.
- [17] S. Tian, B. G. Cangan, S. E. Navarro, A. Beger, C. Duriez, and R. K. Katzschmann, "Multi-tap resistive sensing and fem modeling enables shape and force estimation in soft robots," *IEEE Robotics and Automation Letters*, 2023.
- [18] P. S. Maybeck, "The kalman filter: An introduction to concepts," in Autonomous robot vehicles. Springer, 1990, pp. 194–204.
- [19] J. Z. Sasiadek, "Sensor fusion," Annual Reviews in Control, vol. 26, no. 2, pp. 203–228, 2002.
- [20] H. Wang, M. Totaro, and L. Beccai, "Toward perceptive soft robots: Progress and challenges," Advanced Science, vol. 5, no. 9, p. 1800541, 2018
- [21] D. Kim, S.-H. Kim, T. Kim, B. B. Kang, M. Lee, W. Park, S. Ku, D. Kim, J. Kwon, H. Lee *et al.*, "Review of machine learning methods in soft robotics," *Plos one*, vol. 16, no. 2, p. e0246102, 2021.
- [22] R. L. Truby, C. Della Santina, and D. Rus, "Distributed proprioception of 3d configuration in soft, sensorized robots via deep learning," *IEEE Robotics and Automation Letters*, vol. 5, no. 2, pp. 3299–3306, 2020.
- [23] J. Guo, Z. Li, J.-H. Low, Q. Han, J. L. C.-Y. Chen, Z. Liu, and C.-H. Yeow, "Kirigami-inspired 3d printable soft pneumatic actuators with multiple deformation modes for soft robotic applications," *Soft Robotics*, vol. 10, no. 4, pp. 737–753, 2023.
- [24] O. Kedilioglu, T. M. Bocco, M. Landesberger, A. Rizzo, and J. Franke, "Arucoe: Enhanced aruco marker," in 2021 The 21st International Conference on Control, Automation and Systems (ICCAS). Jeju, Korea: IEEE, 2021, pp. 878–879. [Online]. Available: https://ieeexplore.ieee.org/document/9650050
- [25] Z. Zhang, "A flexible new technique for camera calibration," *IEEE Transactions on Pattern Analysis and Machine Intelligence*, vol. 22, no. 11, pp. 1330–1334, 2000.